Rare Met. (2018) 37(6):480–487
https://doi.org/10.1007/s12598-018-1020-3

RARE METALS
www.editorialmanager.com/rmet

NASICON-structured $Na_{3.1}Zr_{1.95}Mg_{0.05}Si_2PO_{12}$ solid electrolyte for solid-state sodium batteries

Jing Yang, Hong-Li Wan, Zhi-Hua Zhang, Gao-Zhan Liu, Xiao-Xiong Xu, Yong-Sheng Hu, Xia-Yin Yao*

Received: 11 December 2017 / Revised: 5 February 2018 / Accepted: 5 March 2018 / Published online: 2 April 2018

Abstract Using stable inorganic solid electrolyte to replace organic liquid electrolyte could significantly reduce potential safety risks of rechargeable batteries. Na-superionic conductor (NASICON)-structured solid electrolyte is one of the most promising sodium solid electrolytes and can be employed in solid-state sodium batteries. In this work, a NASICON-structured solid electrolyte $Na_{3.1}Zr_{1.95}Mg_{0.05}Si_2PO_{12}$ was synthesized through a facile solid-state reaction, yielding high sodium-ionic conductivity of 1.33×10^{-3} S·cm^{-1} at room temperature. The results indicate that Mg^{2+} is a suitable and economical substitution ion to replace Zr^{4+}, and this synthesis route can be scaled up for powder preparation with low cost. In addition to electrolyte material preparation, solid-state batteries with $Na_{3.1}Zr_{1.95}Mg_{0.05}Si_2PO_{12}$ as electrolyte were assembled. A specific capacity of 57.9 mAh·g^{-1} is maintained after 100 cycles under a current density of 0.5C rate at room temperature. The favorable cycling performance of the solid-state battery suggests that $Na_{3.1}Zr_{1.95}Mg_{0.05}Si_2PO_{12}$ is an ideal electrolyte candidate for solid-state sodium batteries.

Keywords Solid electrolyte; NASICON-type structure; Sodium-ionic conductivity; Solid-state sodium battery

J. Yang, H.-L. Wan, Z.-H. Zhang, G.-Z. Liu, X.-X. Xu, X.-Y. Yao*
Ningbo Institute of Materials Technology and Engineering, Chinese Academy of Sciences, Ningbo 315201, China
e-mail: yaoxy@nimte.ac.cn

H.-L. Wan, Z.-H. Zhang, G.-Z. Liu, Y.-S. Hu
University of Chinese Academy of Sciences, Beijing 100049, China

Y.-S. Hu
Key Laboratory for Renewable Energy Beijing Key Laboratory for New Energy Materials and Devices, Institute of Physics, Chinese Academy of Sciences, Beijing 100190, China

1 Introduction

Renewable energy is of vital importance in the near future due to global energy crisis and worldwide environmental issues. Advanced energy storage systems are required to meet the demands of intermittent energy sources, such as wind and solar power. Owing to their high energy densities and long cycle lives, lithium-ion batteries have been extensively applied in every aspects of society [1, 2]. Nevertheless, as the lithium reserves are limited and unevenly distributed in the crust, it is crucial to find a replacement of lithium before it is depleted [3, 4]. In contrast to lithium, sodium is a naturally abundant element with low cost and low redox potential (− 2.71 V versus standard hydrogen electrode), making sodium-ion batteries an ideal candidate in large-scale energy storage devices [5–10].

However, safety issues related to flammable liquid organic electrolyte remain a serious threat to the application of conventional sodium-ion batteries [11, 12]. Unlike liquid sodium-ion batteries, solid-state sodium batteries with stable nonflammable solid electrolyte can eliminate the safety problems [13, 14], making them as promising power sources for the coming future.

The solid electrolyte is a key component in solid-state sodium batteries, as it conducts the sodium ions between cathode and anode and affects the energy density, cycle life and operating conditions of the battery. Among all possible sodium electrolyte materials, Na-superionic conductor (NASICON)-structured solid electrolyte has been identified as a promising solid electrolyte material due to its high ionic conductivity, good structural stability, wide electrochemical window, relative low cost, as well as versatility [15–17]; thus, it can be applied in high energy density solid-state

batteries. In 1976, Hong et al. discovered the NASICON-structured compound $Na_{1+x}Zr_2Si_xP_{3-x}O_{12}$ ($0 \leq x \leq 3$) [18, 19], which is one of the first reported Na-ion conductors with three-dimensional structure. Since then, $Na_{1+x}Zr_2Si_xP_{3-x}O_{12}$ has been extensively studied to further improve their ionic conducting property. Within this series of compositions, the typical conductivity values at ambient temperature are in the order of 1×10^{-4} S·cm^{-1}, which are obtained for $x = 2$ [20, 21]. In addition, substituting Zr^{4+} with suitable cations such as Sc^{3+}, Hf^{4+} and La^{3+} has been proved to be an efficient way to further enhance the room temperature ionic conductivity of $Na_{1+x}Zr_2Si_xP_{3-x}O_{12}$ compound [21–24].

Although the ionic conductivities of these materials could meet the application requirements, some expensive rare-earth elements are used, and the ionic conductivity needs to be further improved. In this work, Mg^{2+}, an earth-abundant and cost-effective divalent dopant was employed. $Na_{3.1}Zr_{1.95}Mg_{0.05}Si_2PO_{12}$ was synthesized through solid-state reaction and systematically characterized. The results show that Zr^{4+} is partially replaced by low-cost Mg^{2+}, which could enhance the ionic conductivity significantly. The highest room temperature sodium-ion conductivity reaches 1.33×10^{-3} S·cm^{-1}. Solid-state battery with $Na_{3.1}Zr_{1.95}Mg_{0.05}Si_2PO_{12}$ electrolyte pellet was assembled, which exhibited favorable cycling performance at room temperature, proving that $Na_{3.1}Zr_{1.95}Mg_{0.05}Si_2PO_{12}$ could meet the solid-state sodium battery application requirements and is a suitable electrolyte material for high safety energy storage devices.

2 Experimental

2.1 Material synthesis

The NASICON-structured compound $Na_{3.1}Zr_{1.95}Mg_{0.05}Si_2PO_{12}$ was prepared through a facile solid-state reaction method using Na_2CO_3 (99.8%, Aladdin), ZrO_2 (99.99%, Aladdin), MgO (99.9%, Aladdin), SiO_2 (99.99%, Aladdin) and $NH_4H_2PO_4$ (99%, Aladdin) as starting materials. Stoichiometric amounts of starting materials were thoroughly mixed by planetary ball milling in ethanol for 4 h to achieve homogeneous state and then dried in an oven over night. Calcination was performed at 900 °C to release volatile products from starting materials. The calcined power was grounded, followed by planetary ball milling in ethanol for 4 h. The obtained NASICON powder was pressed into pellets with a diameter of 10 mm and further processed through isostatic pressing at 200 MPa. These pellets were then sintered at different temperatures to obtain the final product. The whole sintering process was conducted on a platinum sheet to protect the samples from reacting with the alumina refractory board. For comparison, $Na_3Zr_2Si_2PO_{12}$ was synthesized through the same process as mentioned above in the absence of MgO.

2.2 Material characterization

The phase composition of $Na_{3.1}Zr_{1.95}Mg_{0.05}Si_2PO_{12}$ samples was identified by X-ray diffractometer (XRD, Bruker, D8 Advance, Germany) using Cu Kα radiation in a 2θ range of 10°–80° at a scanning step rate of 2 (°)·min^{-1}. The cross-sectional morphology was observed by field emission scanning electron microscopy (FESEM, Hitachi, S4800, Japan). For electrochemical impedance spectroscopy (EIS) measurements, gold blocking electrodes were sputtered on both sides of as-polished samples. EIS measurements were taken using an impedance analyzer (Solartron 1470E) with an alternating current (AC) signal of 10 mV over the frequency range of 1.0 MHz–0.1 Hz. The data were analyzed by Z-View impedance software. To obtain impedance values at different temperatures, EIS measurements were taken in an environmental chamber at various temperatures, and activation energies were calculated from the temperature dependence of conductivity. Electronic conductivity was examined by direct current (DC) polarization experiment with an applied voltage of 0.01 V, in which gold was sputtered on the surface as blocking electrode. Cyclic voltammetry (CV) measurement was taken at a range of − 0.5 to 6.0 V to determine the electrochemical window of the $Na_{3.1}Zr_{1.95}Mg_{0.05}Si_2PO_{12}$. The densities of the pellet samples were measured with the Archimedes method. The dry weight, wet weight and buoyant weight were recorded after each step, with which the relative densities were calculated and compared.

2.3 Solid-state battery assembling and testing

The solid-state battery was assembled using sodium metal anode, $Na_{3.1}Zr_{1.95}Mg_{0.05}Si_2PO_{12}$ ceramics pellet and $Na_{0.9}Cu_{0.22}Fe_{0.3}Mn_{0.48}O_2$ composite cathode [25] Dense $Na_{3.1}Zr_{1.95}Mg_{0.05}Si_2PO_{12}$ ceramics pellets were obtained through solid-state reaction method as mentioned above. Fine $Na_{0.9}Cu_{0.22}Fe_{0.3}Mn_{0.48}O_2$ powder and conductive additives were mixed together first, then polyvinylidene fluoride (PVDF) organic binder and N-methyl pyrrolidone (NMP) were added to the mixture to obtain the electrode slurry. The slurry was then applied onto the surface of $Na_{3.1}Zr_{1.95}Mg_{0.05}Si_2PO_{12}$ pellet with a doctor blade and dried at 80 °C. A metallic sodium disk was pressed on the other side of $Na_{3.1}Zr_{1.95}Mg_{0.05}Si_2PO_{12}$ pellet and used as anode. Finally, the battery was fabricated by pressing the coated electrolyte pellet and metallic sodium disk. To reduce the interfacial resistance between cathode and electrolyte, one drop liquid electrolyte was added as the

interfacial wetting agent at the cathode side. The liquid electrolyte, which consisted of 1 mol·L^{-1} $NaClO_4$ in propylene carbonate with 5% fluoroethylene carbonate (FEC), was used without further treatment. The whole assemble process was conducted in an argon-filled glove box.

Electrochemical measurements of the fabricated solid-state battery were taken under galvanostatic conditions using a Land-CT2001A battery test system (Jinnuo Wuhan Corp., China). The experiment was carried out at a current of 0.5C (1C = 120 mAh·g^{-1}) in the voltage range of 2.5 to 4.0 V (vs. Na/Na$^+$) at 25 °C.

3 Results and discussion

3.1 Characterization of NASICON solid electrolytes

XRD patterns of the obtained samples and $Na_3Zr_2Si_2PO_{12}$ are shown in Fig. 1. Four different sintering temperatures were employed in order to determine the optimum sintering temperature, which are 1100, 1200, 1225 and 1250 °C, respectively. The NASICON-type phase $Na_3Zr_2Si_2PO_{12}$ is found to be the major crystalline phase of all samples, suggesting that this solid-state synthesize procedure could synthesize NASICON-structured compound effectively. The results also indicate that Mg^{2+} substitution at low concentration has little effect on crystalline structure, as no difference could be observed between major crystalline phase and that of $Na_3Zr_2Si_2PO_{12}$. Apart from NASICON-type phase, small diffraction peaks related to ZrO_2 were detected. The peak intensities of ZrO_2 peaks increase with temperature, showing that the presence of ZrO_2 is originated from the decomposition of major crystalline phase at elevated temperatures [26–29]. Actually, the presence of ZrO_2 impurity in NASICON-structured solid electrolyte material is a common phenomenon, especially in the solid electrolytes prepared through solid-state reactions [27, 28, 30, 31]. Moreover, $Na_3Zr_2Si_2PO_{12}$-based materials prepared with less ZrO_2 impurity through a sol–gel method were reported [32, 33]; however, no significant improvement in conductivity is achieved for these materials.

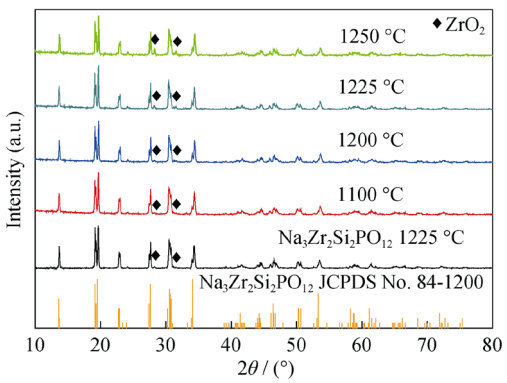

Fig. 1 XRD patterns of $Na_3Zr_2Si_2PO_{12}$ and $Na_{3.1}Zr_{1.95}Mg_{0.05}Si_2PO_{12}$ samples sintered at different temperatures

To investigate the effects of sintering temperatures on the microstructure, cross-sectional morphologies of $Na_{3.1}Zr_{1.95}Mg_{0.05}Si_2PO_{12}$ samples sintered at different temperatures were further investigated by FESEM, as shown in Fig. 2. In Fig. 2a, obvious pores distributed in grain boundary regions could be observed, suggesting that the sintering temperature is too low for the densification of the sample. By contrast, no apparent defect could be detected in Fig. 2c, d. It is worth noticing that samples sintered above 1100 °C possess much denser microstructure compared with their counterpart sintered at 1100 °C. This phenomenon proves that proper sintering temperature could reduce the pores within the structure, attributing to favorable contact between the grains and larger grain boundary contact area.

As sintering temperature has significant influences on phase composition and microstructure, the electrical property could be affected as well. Figure 3 exhibits the impedance profiles measured at 25 °C of $Na_{3.1}Zr_{1.95}Mg_{0.05}Si_2PO_{12}$ samples sintered at different temperatures. All impedance spectra contain a semicircle which is attributed to the grain boundary resistance (R_{gb}). The intercept of the semicircle with the real axis at high frequency represents the bulk resistance (R_b). The total resistance (R_t) equals with the sum of R_{gb} and R_b. It is observed that R_t value decreases drastically as the sintering temperature increases from 1100 to 1200 °C. Though both R_{gb} and R_b value decrease in this process, however, the change in R_{gb} value is the major influence factor. The sample sintered at 1225 °C exhibits the lowest R_t value among all samples. R_t value is elevated with further increase in sintering temperature. The temperature dependence of total ionic conductivity (σ_t) of $Na_{3.1}Zr_{1.95}Mg_{0.05}Si_2PO_{12}$ samples is demonstrated in Fig. 4. The calculated conductivity values of all samples show good linear fitting results, indicating that no phase transformation took place during the measuring process. The activation energies were calculated from Arrhenius plots, using the conductivity values measured in the temperature range from − 10 to 100 °C. To unravel the mechanism that leads to the changes in conductivity values, the relative densities of these $Na_{3.1}Zr_{1.95}Mg_{0.05}Si_2PO_{12}$ pellets were measured. The calculated values of bulk conductivity, grain boundary conductivity, total conductivity, activation energy and relative density of $Na_{3.1}Zr_{1.95}Mg_{0.05}Si_2PO_{12}$ samples sintered at different temperatures are listed in Table 1. It could be concluded that the optimum sintering temperature is 1225 °C, and the sample sintered at this temperature possesses the highest ionic conductivity and relative density as well as the lowest activation energy. The highest ionic conductively among all sample is 1.33 × 10^{-3} S·cm^{-1}.

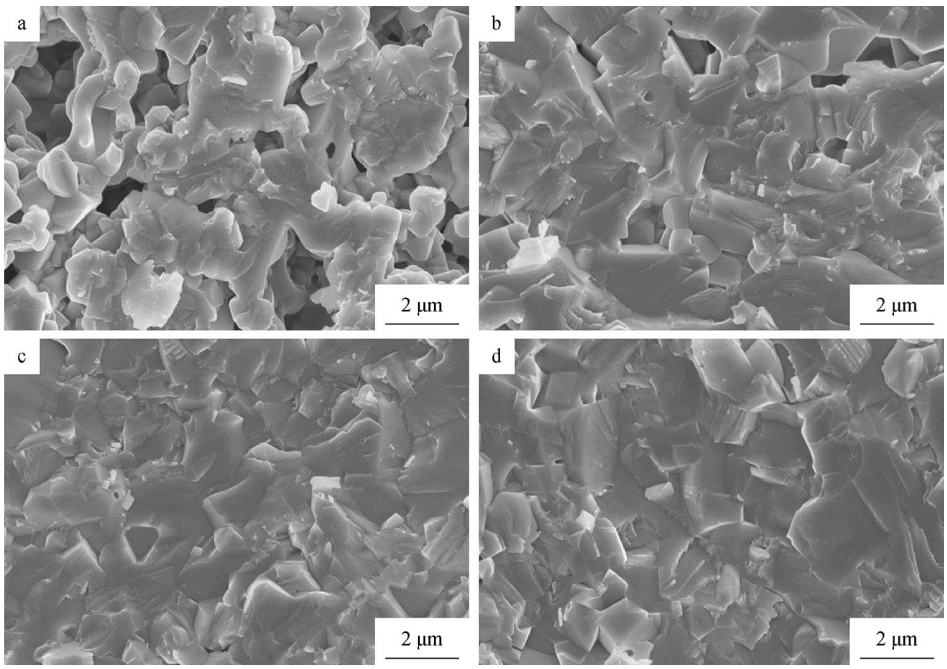

Fig. 2 Cross-sectional FESEM images of $Na_{3.1}Zr_{1.95}Mg_{0.05}Si_2PO_{12}$ samples sintered at different temperatures: **a** 1100 °C, **b** 1200 °C, **c** 1225 °C and **d** 1250 °C

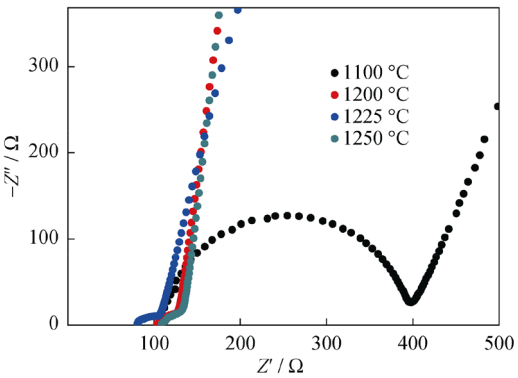

Fig. 3 Impedance profiles measured at 25 °C of $Na_{3.1}Zr_{1.95}Mg_{0.05}Si_2PO_{12}$ samples sintered at different temperatures, where Z' and Z'' representing real and imaginary parts of impedance value, respectively

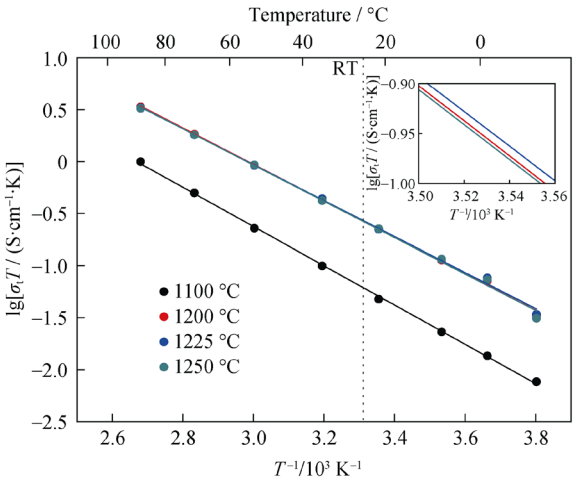

Fig. 4 Temperature dependence of total ionic conductivity of $Na_{3.1}Zr_{1.95}Mg_{0.05}Si_2PO_{12}$ samples sintered at different temperatures

The ionic conductivity and relative density increase as the sintering temperature elevates from 1100 to 1225 °C. As the temperature continues to rise to 1250 °C, the ionic conductivity and relative density decrease. On the contrary, the activation energy shows an opposite trend, which is in good accordance with conductivity values.

In contrast, the $Na_3Zr_2Si_2PO_{12}$ samples deliver lower conductivities and densities, as shown in Table 1. Therefore, these results confirm that Mg^{2+} substitution could effectively enhance the ion conducting capability. The addition of Mg^{2+} elevates the concentration of Na^+ in the formula and induces dense microstructure, which are helpful for ion conduction.

The relationship between ionic conductivity, activation energy (E_a), density and sintering temperature of $Na_{3.1}Zr_{1.95}Mg_{0.05}Si_2PO_{12}$ and $Na_3Zr_2Si_2PO_{12}$ samples is exhibited in Fig. 5. It is worth noticing that the total conductivity of $Na_{3.1}Zr_{1.95}Mg_{0.05}Si_2PO_{12}$ samples drastically increases from 3.39×10^{-4} to 1.01×10^{-3} S·cm^{-1} when sintering temperature increases from 1100 to 1200 °C, which could be attributed to the increase in grain boundary conductivity. The rise of grain boundary conductivity indicates that the sintering temperature mainly affects the grain boundary region, which could be further confirmed

Table 1 Bulk conductivity, grain boundary conductivity, total conductivity, activation energy and relative density of $Na_{3.1}Zr_{1.95}Mg_{0.05}Si_2PO_{12}$ and $Na_3Zr_2Si_2PO_{12}$ samples sintered at different temperatures

Samples	Bulk conductivity/ ($S \cdot cm^{-1}$)	Grain boundary conductivity/ ($S \cdot cm^{-1}$)	Total conductivity/ ($S \cdot cm^{-1}$)	Activation energy/ eV	Relative density/ %
$Na_{3.1}Zr_{1.95}Mg_{0.05}Si_2PO_{12}$					
1100 °C	1.25×10^{-3}	4.66×10^{-4}	3.39×10^{-4}	0.38	74.42
1200 °C	1.54×10^{-3}	2.89×10^{-3}	1.01×10^{-3}	0.35	93.61
1225 °C	2.06×10^{-3}	3.75×10^{-3}	1.33×10^{-3}	0.34	97.82
1250 °C	1.48×10^{-3}	2.54×10^{-3}	9.37×10^{-4}	0.35	95.65
$Na_3Zr_2Si_2PO_{12}$					
1100 °C	5.11×10^{-4}	4.88×10^{-4}	2.50×10^{-4}	0.39	70.05
1200 °C	5.88×10^{-4}	4.53×10^{-4}	2.56×10^{-4}	0.38	73.40
1225 °C	6.47×10^{-4}	4.16×10^{-4}	2.53×10^{-4}	0.38	78.84
1250 °C	6.55×10^{-4}	3.24×10^{-4}	2.17×10^{-4}	0.41	84.02

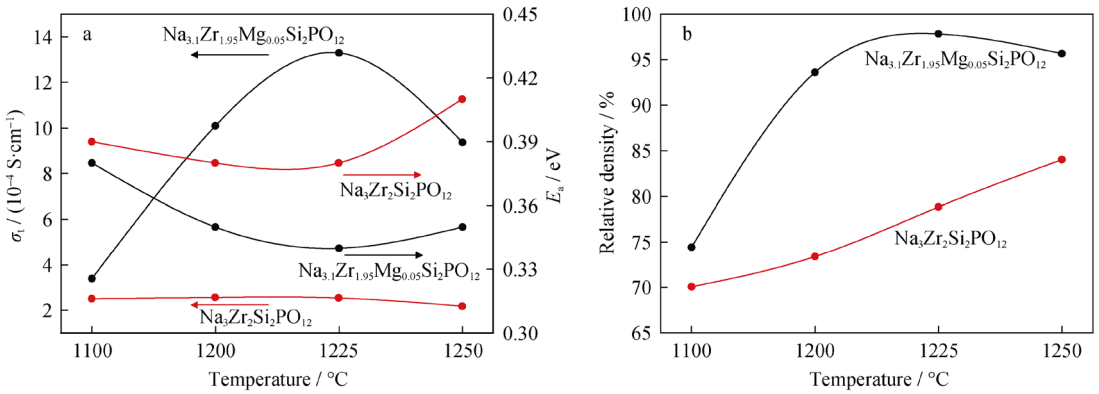

Fig. 5 **a** Total conductivity and activation energy versus sintering temperature for $Na_{3.1}Zr_{1.95}Mg_{0.05}Si_2PO_{12}$ and $Na_3Zr_2Si_2PO_{12}$ samples; **b** dependence of relative density on sintering temperature for $Na_{3.1}Zr_{1.95}Mg_{0.05}Si_2PO_{12}$ and $Na_3Zr_2Si_2PO_{12}$ samples

by FESEM observations. Owing to the increase in sintering temperature, the pores between the grains vanish. Hence, the migration of sodium ions at grain boundary region is promoted, leading to higher grain boundary conductivity and total conductivity. This could also be proved by the improvement in relative density. In addition, samples with higher Mg^{2+} substitution level were also prepared, and the ionic conductivities were evaluated. $Na_{3.2}Zr_{1.9}Mg_{0.1}Si_2PO_{12}$ sample, prepared through the same method and sintered at 1225 °C, shows a room temperature ionic conductivity of 1.23×10^{-3} $S \cdot cm^{-1}$, which is slightly lower than that of $Na_{3.1}Zr_{1.95}Mg_{0.05}Si_2PO_{12}$ sample.

From the EIS results above, the total conductivity of $Na_{3.1}Zr_{1.95}Mg_{0.05}Si_2PO_{12}$ sample sintered at 1225 °C is more than 1×10^{-3} $S \cdot cm^{-1}$ and could meet the application requirements as electrolyte material. However, the electronic conductivity of $Na_{3.1}Zr_{1.95}Mg_{0.05}Si_2PO_{12}$ also needs to be determined, as electronic conduction through the electrolyte in the battery would lead to short circuit and self-discharge. Figure 6 shows the result of DC polarization measurement of sintered $Na_{3.1}Zr_{1.95}Mg_{0.05}Si_2PO_{12}$ pellet at room temperature. The electron conductivity is calculated to be 1.12×10^{-7} $S \cdot cm^{-1}$; thus, the sodium-ion transference number is close to 1, $t_{Na^+}=(\sigma_t - \sigma_e)/\sigma_t = 0.9999$, where t_{Na^+}, σ_t and σ_e are sodium-ion transference number, total conductivity and electron conductivity, respectively, suggesting that sodium ion is the dominant charge carrier in $Na_{3.1}Zr_{1.95}Mg_{0.05}Si_2PO_{12}$. Besides high ionic conductivity, the solid electrolyte materials also require a wide and stable electrochemical window to remain stable during charge–discharge process. The electrochemical stability of $Na_{3.1}Zr_{1.95}Mg_{0.05}Si_2PO_{12}$ against metallic sodium was analyzed through CV measurement using a Na/$Na_{3.1}Zr_{1.95}Mg_{0.05}Si_2PO_{12}$/Au cell, as demonstrated in Fig. 7. Clearly, except two peaks related to sodium dissolution and sodium deposition in the low potential range, no other peaks are observed up to 6 V (vs. Na/Na^+), showing that $Na_{3.1}Zr_{1.95}Mg_{0.05}Si_2PO_{12}$ is stable in direct contact with metallic sodium within the tested voltage range. Therefore, $Na_{3.1}Zr_{1.95}Mg_{0.05}Si_2PO_{12}$

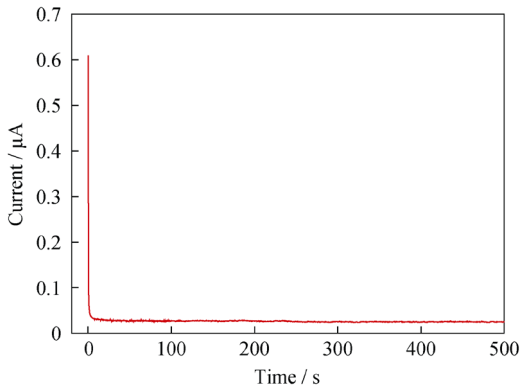

Fig. 6 DC polarization curve of $Na_{3.1}Zr_{1.95}Mg_{0.05}Si_2PO_{12}$ sample

material possesses a wide electrochemical window up to 6 V (vs. Na/Na^+), which is sufficient to most cathode materials. The wide electrochemical window of electrolyte material indicates the possibility of applying high voltage cathode materials in the battery; thus, the energy density of the battery using $Na_{3.1}Zr_{1.95}Mg_{0.05}Si_2PO_{12}$ as electrolyte could be increased. Based on the results of ionic and electronic conductivity as well as electrochemical window, it is viable to employ $Na_{3.1}Zr_{1.95}Mg_{0.05}Si_2PO_{12}$ as electrolyte material in solid-state batteries.

3.2 Application in solid-state battery

As described in the experimental section, $Na_{3.1}Zr_{1.95}Mg_{0.05}Si_2PO_{12}$ pellet was sandwiched between $Na_{0.9}Cu_{0.22}Fe_{0.3}Mn_{0.48}O_2$ cathode and metallic sodium anode. The electrochemical performance of the solid-state battery operated under a current density of 0.5C after two activation cycles at room temperature is illustrated in Fig. 8. The cell can deliver a reversible capacity of 71.9 $mAh \cdot g^{-1}$. After 100 cycles, the discharge capacity remains at 57.9 $mAh \cdot g^{-1}$, showing a capacity retention ratio of 80.5% at 0.5C. It can be inferred that the highly conducting $Na_{3.1}Zr_{1.95}Mg_{0.05}Si_2PO_{12}$ pellet leads to the satisfactory cycling performance of the solid-state battery.

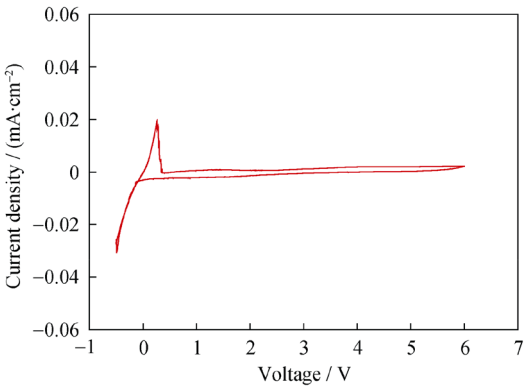

Fig. 7 Cyclic voltammetry of $Na_{3.1}Zr_{1.95}Mg_{0.05}Si_2PO_{12}$ with a $Na/Na_{3.1}Zr_{1.95}Mg_{0.05}Si_2PO_{12}/Au$ cell from − 0.5 to 6.0 V

In solid-state batteries, it is crucial to investigate the ion diffusion kinetics at the interfaces, which affects the electrochemical performance of the batteries. Sodium-ion transfer within the electrolyte and through the interfaces between electrode and electrolyte under different cycles at room temperature was studied by EIS measurements, as depicted in Fig. 9. A semicircle and a line are observed in the impedance spectra. The intercept of semicircle at high frequency is mainly ascribed to the resistance of $Na_{3.1}Zr_{1.95}Mg_{0.05}Si_2PO_{12}$ pellet, while the semicircle appeared at lower frequency is attributed to the charge-transfer resistance, including $Na_{3.1}Zr_{1.95}Mg_{0.05}Si_2PO_{12}/Na$ interface and $Na_{3.1}Zr_{1.95}Mg_{0.05}Si_2PO_{12}/Na_{0.9}Cu_{0.22}Fe_{0.3}Mn_{0.48}O_2$ interface [34–36]. Obviously, the impedance of the solid-state battery is mainly arising from the interfacial resistance. As known, in the traditional batteries, the cathode and anode materials are immersed in liquid electrolyte, which facilities the ion transport. However, for solid-state batteries, the interfacial contact is basically point to point contact [14], showing much lower transfer rate of charge carriers and leading to larger interfacial impedance. It can be observed that the battery exhibits good cycling stability as the impedance profiles are almost changeless after 100 cycles, showing that the battery could remain stable and operate without undesirable side reactions at room temperature. Compared with the resistance of $Na_{3.1}Zr_{1.95}Mg_{0.05}Si_2PO_{12}$ electrolyte, the interfacial resistance value is much larger. As the interfacial resistance could significantly affect the cyclic performance and rate performance, it is suggested that the interfaces within solid-state batteries need to be further improved in ion conduction capability to achieve superior battery performances.

4 Conclusion

In summary, a NASICON-type sodium-ion conducting solid electrolyte $Na_{3.1}Zr_{1.95}Mg_{0.05}Si_2PO_{12}$ was synthesized through facile solid-state reaction and systematically characterized. The highest total conductivity of 1.33×10^{-3} $S \cdot cm^{-1}$ at room temperature is obtained for $Na_{3.1}Zr_{1.95}Mg_{0.05}Si_2PO_{12}$ pellet sintered at 1225 °C, proving that the ionic conductivity could be effectively enhanced by the substitution of Mg^{2+}. Through FESEM observation and the result of relative density calculation, it is confirmed that proper sintering temperature could reduce the number of pores in grain boundary area, resulting in higher grain boundary conductivity and higher density. The electron conductivity of the sample is negligible with respect to the ionic conductivity, showing that the sample is a pure ionic conductor. A wide electrochemical window up to 6 V vs. Na/Na^+ of the sample is observed. Solid-state battery with $Na_{0.9}Cu_{0.22}Fe_{0.3}Mn_{0.48}O_2$ cathode and metallic sodium anode was assembled, and the battery showed

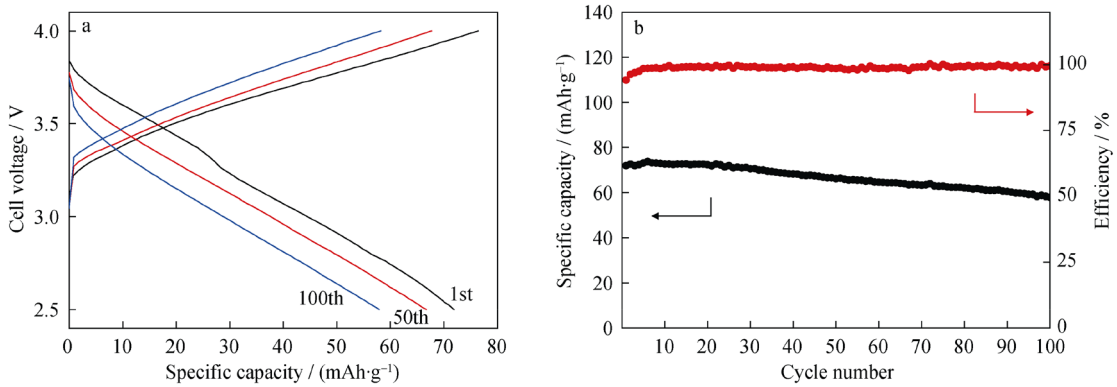

Fig. 8 **a** Charge–discharge curve of solid-state battery operated at room temperature; **b** cycling performance of solid-state battery operated at room temperature

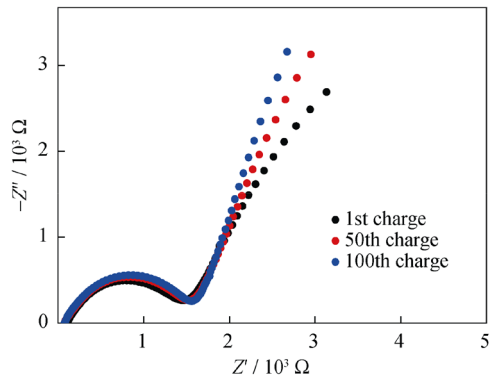

Fig. 9 Impedance profiles after different cycles of solid-state battery assembled with $Na_{3.1}Zr_{1.95}Mg_{0.05}Si_2PO_{12}$ electrolyte pellet

favorable cycling performance in terms of high capacity and cycle stability under a current rate of 0.5C at room temperature. The outstanding electrochemical performance could be ascribed to the superior ionic conductivity of $Na_{3.1}Zr_{1.95}Mg_{0.05}Si_2PO_{12}$ material. The cycling performance of the solid-state battery suggests that $Na_{3.1}Zr_{1.95}Mg_{0.05}Si_2PO_{12}$ could be potentially extended to other high energy density solid-state battery systems.

Acknowledgements This work is financially supported by the National Key Research and Development Program of China (No. 2016YFB0100105), Strategic Priority Program of the Chinese Academy of Sciences (No. XDA09010203), Zhejiang Provincial Natural Science Foundation of China (Nos. LD18E020004, LY18E020018 and LY18E030011) and the Youth Innovation Promotion Association CAS (No. 2017342).

References

[1] Goodenough JB, Kim Y. Challenges for rechargeable Li batteries. Chem Mater. 2009;22(3):587.
[2] Kim Y, Kim H, Park S, Seo I, Kim Y. Na ion-conducting ceramic as solid electrolyte for rechargeable seawater batteries. Electrochim Acta. 2016;191:1.
[3] Zhao C, Lu Y, Li Y, Jiang L, Rong X, Hu YS, Li H, Chen L. Novel methods for sodium-ion battery materials. Small Methods. 2017;1(5):1600063.
[4] Palomares V, Serras P, Villaluenga I, Hueso KB, Carretero-Gonzalez J, Rojo T. Na-ion batteries, recent advances and present challenges to become low cost energy storage systems. Energ Environ Sci. 2012;5(3):5884.
[5] Hueso KB, Armand M, Rojo T. High temperature sodium batteries: status, challenges and future trends. Energ Environ Sci. 2013;6(3):734.
[6] Song S, Duong HM, Korsunsky AM, Hu N, Lu L. A Na^+ superionic conductor for room-temperature sodium batteries. Sci Rep. 2016;6:32330.
[7] Bui KM, Dinh VA, Okada S, Ohno T. Na-ion diffusion in a NASICON-type solid electrolyte: a density functional study. Phys Chem Chem Phys. 2016;18(39):27226.
[8] Song W, Wu Z, Chen J, Lan Q, Zhu Y, Yang Y, Pan C, Hou H, Jing M, Ji X. High-voltage NASICON sodium ion batteries: merits of fluorine insertion. Electrochim Acta. 2014;146:142.
[9] Luo W, Gaumet JJ, Mai LQ. Antimony-based intermetallic compounds for lithium-ion and sodium-ion batteries: synthesis, construction and application. Rare Met. 2017;36(5):321.
[10] Liu GQ, Li Y, Du YL, Wen L. Synthesis and properties of $Na_{0.8}Ni_{0.4}Mn_{0.6}O_2$ oxide used as cathode material for sodium ion batteries. Rare Met. 2017;36(12):977.
[11] Kim JG, Son B, Mukherjee S, Schuppert N, Bates A, Kwon O, Choi MJ, Chung HY, Park S. A review of lithium and non-lithium based solid state batteries. J Power Sour. 2015;282:299.
[12] Vignarooban K, Kushagra R, Elango A, Badami P, Mellander BE, Xu X, Tucker TG, Nam C, Kannan AM. Current trends and future challenges of electrolytes for sodium-ion batteries. Int J Hydrogen Energ. 2016;41(4):2829.
[13] Che H, Chen S, Xie Y, Wang H, Amine K, Liao XZ, Ma ZF. Electrolyte design strategies and research progress for room-temperature sodium-ion batteries. Energ Environ Sci. 2017;10(5):1075.
[14] Zhou W, Li Y, Xin S, Goodenough JB. Rechargeable sodium all-solid-state battery. ACS Central Sci. 2017;3(1):52.
[15] Jian Z, Hu YS, Ji X, Chen W. NASICON-structured materials for energy storage. Adv Mater. 2017;29(20):1601925.
[16] Fergus JW. Ion transport in sodium ion conducting solid electrolytes. Solid State Ionics. 2012;227:102.
[17] Anantharamulu N, Rao KK, Rambabu G, Kumar BV, Radha V, Vithal M. A wide-ranging review on Nasicon type materials. J Mater Sci. 2011;46(9):2821.
[18] Goodenough JB, Hong HYP, Kafalas JA. Fast Na^+-ion transport in skeleton structures. Mater Res Bull. 1976;11(2):203.

[19] Hong HYP. Crystal structures and crystal chemistry in the system $Na_{1+x}Zr_2Si_xP_{3-x}O_{12}$. Mater Res Bull. 1976;11(2):173.
[20] Kim JJ, Yoon K, Park I, Kang K. Progress in the development of sodium-ion solid electrolytes. Small Methods. 2017;1(10): 1700219.
[21] Guin M, Tietz F. Survey of the transport properties of sodium superionic conductor materials for use in sodium batteries. J Power Sour. 2015;273:1056.
[22] Ma Q, Guin M, Naqash S, Tsai CL, Tietz F, Guillon O. Scandium-substituted $Na_3Zr_2(SiO_4)_2(PO_4)$ prepared by a solution-assisted solid-state reaction method as sodium-ion conductors. Chem Mater. 2016;28(13):4821.
[23] Guin M, Dashjav E, Kumar CMN, Tietz F, Guillon O. Investigation of crystal structure and ionic transport in a scandium-based NASICON material by neutron powder diffraction. Solid State Sci. 2017;67:30.
[24] Vogel EM, Cava RJ, Rietman E. Na^+ ion conductivity and crystallographic cell characterization in the Hf-nasicon system $Na_{1+x}Hf_2Si_xP_{3-x}O_{12}$. Solid State Ionics. 1984;14(1):1.
[25] Mu L, Xu S, Li Y, Hu YS, Li H, Chen L, Huang X. Prototype sodium-ion batteries using an air-stable and Co/Ni-free O3-layered metal oxide cathode. Adv Mater. 2015;27(43):6928.
[26] Ruan Y, Song S, Liu J, Liu P, Cheng B, Song X, Battaglia V. Improved structural stability and ionic conductivity of $Na_3Zr_{2-}Si_2PO_{12}$ solid electrolyte by rare earth metal substitutions. Ceram Int. 2017;43(10):7810.
[27] Park H, Jung K, Nezafati M, Kim CS, Kang B. Sodium ion diffusion in Nasicon ($Na_3Zr_2Si_2PO_{12}$) solid electrolytes: effects of excess sodium. ACS Appl Mater Inter. 2016;8(41):27814.
[28] Khakpour Z. Influence of M: Ce^{4+}, Gd^{3+} and Yb^{3+} substituted $Na_{3+x}Zr_{2-x}M_xSi_2PO_{12}$ solid NASICON electrolytes on sintering, microstructure and conductivity. Electrochim Acta. 2016;196:337.
[29] Bell NS, Edney C, Wheeler JS, Ingersoll D, Spoerke ED. The influences of excess sodium on low-temperature NaSICON synthesis. J Am Ceram Soc. 2014;97(12):3744.
[30] Lee JS, Chang CM, Lee YIL, Lee JH, Hong SH. Spark plasma sintering (SPS) of NASICON ceramics. J Am Ceram Soc. 2004; 87(2):305.
[31] Noi K, Suzuki K, Tanibata N, Hayashi A, Tatsumisago M. Liquid-phase sintering of highly Na^+ ion conducting $Na_3Zr_{2-}Si_2PO_{12}$ ceramics using Na_3BO_3 additive. J Am Ceram Soc. 2017;101(3):1255.
[32] Shimizu Y, Ushijima T. Sol–gel processing of NASICON thin film using aqueous complex precursor. Solid State Ionics. 2000; 132(1–2):143.
[33] Guin M, Tietz F, Guillon O. New promising NASICON material as solid electrolyte for sodium-ion batteries: correlation between composition, crystal structure and ionic conductivity of $Na_{3+x}Sc_2Si_xP_{3-x}O_{12}$. Solid State Ionics. 2016;293:18.
[34] Zhang QQ, Ding F, Sun WB, Sang L. Preparation of LAGP/P(VDF-HFP) polymer electrolytes for Li-ion batteries. RSC Adv. 2015;5(80):65395.
[35] Yoshima K, Harada Y, Takami N. Thin hybrid electrolyte based on garnet-type lithium-ion conductor $Li_7La_3Zr_2O_{12}$ for 12 V-class bipolar batteries. J Power Sour. 2016;302:283.
[36] Zhang J, Zhao J, Yue L, Wang Q, Chai J, Liu Z, Zhou X, Li H, Guo Y, Cui G, Chen L. Safety-reinforced poly(propylene carbonate)-based all-solid-state polymer electrolyte for ambient-temperature solid polymer lithium batteries. Adv Energy Mater. 2015;5(24):1501082.